



Article

Fully Developed Opposing Mixed Convection Flow in the Inclined Channel Filled with a Hybrid Nanofluid

Xiangcheng You * and Shiyuan Li

College of Petroleum Engineering, China University of Petroleum-Beijing, Beijing 102249, China;
lishiyuan1983@cup.edu.cn

* Correspondence: xcyou@cup.edu.cn

Abstract: This paper studies the convective heat transfer of a hybrid nanofluid in the inclined channel, whose walls are both heated by the uniform heat flux. The governing ordinary differential equations are made nondimensional and solved analytically, in which explicit distributions of velocity, temperature and pressure are obtained. The effects of flow reversal, wall skin friction and Nusselt number with the hybrid nanofluid depend on the nanoparticle volume fractions and pressure parameters. The obtained results indicate that the nanoparticle volume fractions play a key role in delaying the occurrence of the flow reversal. The hybrid nanofluids hold more delayed range than conventional nanofluids, which is about 2.5 times that of nanofluids. The calculations have been compared with the base fluid, nanofluid and two kinds of hybrid models (type II and type III). The hybrid model of type III is useful and simplified in that it omits the nonlinear terms due to the interaction of different nanoparticle volumetric fractions, with the relative error less than 3%. More results are discussed in the results section below.



Citation: You, X.; Li, S. Fully Developed Opposing Mixed Convection Flow in the Inclined Channel Filled with a Hybrid Nanofluid. *Nanomaterials* **2021**, *11*, 1107. <https://doi.org/10.3390/nano11051107>

Academic Editors: Hang Xu and Gozde Tutuncuoglu

Received: 04 April 2021

Accepted: 21 April 2021

Published: 25 April 2021

Publisher's Note: MDPI stays neutral with regard to jurisdictional claims in published maps and institutional affiliations.



Copyright: © 2021 by the authors. Licensee MDPI, Basel, Switzerland. This article is an open access article distributed under the terms and conditions of the Creative Commons Attribution (CC BY) license (<https://creativecommons.org/licenses/by/4.0/>).

Keywords: hybrid nanofluid; mixed convection; inclined channel; flow reversal

1. Introduction

Research on mixed convection induced flow is increasingly interested in many engineering applications, such as in heat exchangers, chemical processing equipment, transport of heated or cooled fluids, solar power collectors, microelectronic cooling and so on. Furthermore, the mixed convection flow through a channel has received a great deal of attention [1–5] in literature. However, most of the previous studies have focused on the horizontal or vertical configuration and mixed convection in inclined geometries has been studied less. Thus, it is worthwhile to explore the flow on the inclined flat plate at various angles which is often come across in engineering devices, such as solar water heaters, inclination/acceleration sensors and so on. Bohne et al. [6] investigated superposed free and forced convection in an internally heated concentric annulus in vertical, inclined and horizontal position with experiments. Lavine [7] presented an exact solution of fully developed, laminar flow between inclined parallel plates with a uniform wall heat flux boundary condition. Wang [8] studied numerically with fully developed opposing mixed convection in an inclined channel that had discrete heating on the bottom and was insulated on the top. Barletta et al. [9] researched analytically the fully developed laminar mixed convection with viscous dissipation in an inclined channel with prescribed wall temperatures. Aydin et al. [10] investigated MHD mixed convective heat transfer flow about an inclined plate. Cimpean [11] studied the steady fully developed mixed convection flow of a nanofluid in a channel filled with a porous medium. You et al. [12] presented analysis of fully developed opposing mixed convection flow in an inclined channel filled by a nanofluid. Goyal et al. [13] examined numerically natural convective boundary layer flow of a nanofluid past a heated inclined plate in the presence of magnetic field and found that the thermal boundary layer thickness increased with strengthening the value of inclination angle parameter. Rafique et al. [14] studied numerically on micropolar nanofluid flow over an inclined

surface by means of Keller-Box method. Khademi et al. [15] studied numerical analysis of mixed convection flow of nanofluid over an inclined flat plate embedded in a porous medium in the presence of a transverse magnetic field. Anuar et al. [16] presented work explored the heat transfer and boundary layer flow of a hybrid nanofluid past an inclined stretching/shrinking sheet with suction and buoyancy force effects.

It is well-known that nanofluids have been applied to problems with the thermal properties of heat transfer fluids. The nanofluids were first researched by Choi and Eastman [17]; they are kinds of suspended nanoparticles in the base fluid, such as ethylene glycol, oil or water. The properties of the nanofluids are higher than the base fluid, such as viscosity, diffusion coefficient, heat transfer rate and thermal conductivity [18–22]. Nanofluids can be used in microchip cooling, nuclear reactor, industrial cooling, sensing, drug delivery, nanomedicine, the oil recovery process and so on [23,24]. However, hybrid nanofluids are composed of two different nanoparticles dispersed in the base fluid, which have better thermophysical properties and rheological behavior along with improved heat transfer properties [25–27]. In recent years, many scientists and researchers have been attracted to investigating real-world heat transfer problems with hybrid nanofluids [28–30]. Obviously, it is necessary to study the mechanisms of hybrid nanofluids that contribute to the heat transfer enhancement.

Motivated and based on the literature discussed above, the main aim of this paper is to study the fully developed mixed convection flow in the inclined channel filled with a hybrid nanofluid, which employs simply homogeneous model proposed by Maïga et al. [31]. In this study, hybrid nanofluid is formed by suspending two different nanoparticles, which are copper and alumina, in the base fluid. The governing equations with boundary conditions are solved analytically that have never been reported before based on the literature survey. The model analyses the hybrid nanofluid behavior by comprising the nanoparticles solid volume fractions, which using two kinds of hybrid models (type II and type III). The result shows that the hybrid model of type III is useful and simplified that omits the nonlinear terms due to the interaction of different nanoparticle volumetric fractions. Besides, the effects of the main physical parameters are discussed respectively, such as the nondimensional pressure parameter P_1, P_2 , the nanoparticle volume fractions ϕ_1, ϕ_2 , the velocity profile $U(Y)$, the temperature profile $\theta - \theta_b$, the average wall friction $C_f Re$ and the average Nusselt number \overline{Nu} ; these are illustrated graphically. The hybrid nanofluids hold better thermophysical properties than conventional nanofluids based on the results.

2. Mathematical Model

Consider the steady mixed convection flow, which is driven by a buoyancy force and an external pressure gradient between two paralleled long inclined plane walls filled with a hybrid nanofluid and separated by a distance L . Figure 1 shows the sketch of system and the coordinate axes, where x and y axes are measured along the lower plane of the channel oriented in the downward direction, y axis is in the normal to the lower plane, q is the constant wall heat flux, g is the acceleration due to gravity and γ is the inclination angle of the channel. The velocity field is given in the case by $\mathbf{v}(u, 0)$, then the continuity equation reduces to $\partial u / \partial x = 0$ and implies $u = u(y)$. Following Lavine [7] and using the hybrid nanofluid model, the momentum balance and energy equations according to the Boussinesq approximation are written by

$$\frac{\partial p}{\partial x} = -(\rho\beta)_{hnf} g(T - T_0) \sin \gamma + \mu_{hnf} \frac{d^2 u}{dy^2}, \quad (1)$$

$$\frac{\partial p}{\partial y} = (\rho\beta)_{hnf} g(T - T_0) \cos \gamma, \quad (2)$$

$$u \frac{\partial T}{\partial x} = \alpha_{hnf} \frac{\partial^2 T}{\partial y^2}, \quad (3)$$

subject to the boundary conditions

$$u(0) = 0, \quad u(L) = 0, \quad -\left(\frac{\partial T}{\partial y}\right)\bigg|_{y=0} = \left(\frac{\partial T}{\partial y}\right)\bigg|_{y=L} = 1. \quad (4)$$

The mass flow rate is assumed as a prescribed quantity of this channel flow study, then the following average fluid velocity in the section will be prescribed as

$$\bar{u} = \int_0^L u(y) dy. \quad (5)$$

Here u is the velocity component along the x axis, \bar{u} is the average velocity, T is the temperature of the hybrid nanofluid, T_0 is the constant reference temperature, p is the fluid thermodynamic pressure and g is the gravitational acceleration. The physical quantities in Equations (1)–(3) are ϕ_1, ϕ_2 is the nanoparticle volume fractions, $\beta_f, \beta_{n1}, \beta_{n2}$ are the coefficients of thermal expansion of the base fluid and nanofluid respectively, $\rho_f, \rho_{n1}, \rho_{n2}$ are the densities of the base fluid and nanofluid, μ_{hmf} is the viscosity of the hybrid nanofluid and α_{hmf} is the thermal diffusivity of the hybrid nanofluid, μ_f is the dynamic viscosity of the base fluid and its expression has been proposed by Brinkman [32], k_{hmf} is the thermal conductivity of the hybrid nanofluid, k_f, k_{n1}, k_{n2} are the thermal conductivities of the base fluid and nanofluid, $(\rho C_p)_{hmf}$ is the heat capacitance of the hybrid nanofluid. Note that the expression (5) is restricted to spherical nanoparticles where it does not account for other shapes of nanoparticles. The thermophysical properties of the base fluid, nanofluid and hybrid nanofluid are given in Tables 1–4, referring to references [33–37].

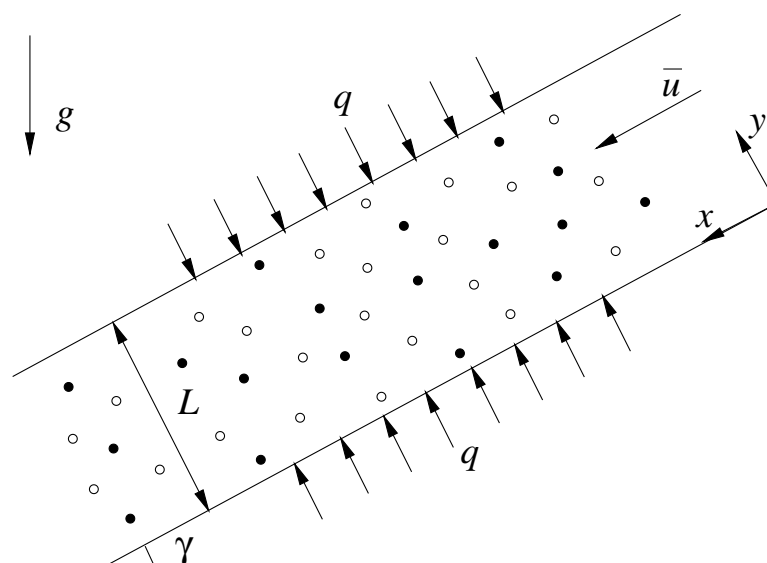


Figure 1. Physical configuration and coordinate system.

Table 1. Thermophysical properties of nanoparticles and water [33].

Physical Properties	Cu	Al_2O_3	H_2O
ρ (kg/m ³)	8933	3970	997.1
C_p (J/kg K)	385	765	4179
k (W/mK)	400	40	0.613
$\alpha \times 10^7$ (m ² /s)	11,163.1	131.7	1.47
$\beta \times 10^{-5}$ (1/K)	1.67	0.85	21

Table 2. Thermophysical properties of nanofluid (type I) [34].

Properties	Nanofluid
Density	$\rho_{nf} = (1 - \phi_1)\rho_f + \phi_1(\rho\beta)_{n1}$
Thermal expansion coefficient	$(\rho\beta)_{nf} = (1 - \phi_1)(\rho\beta)_f + \phi_1(\rho\beta)_{n1}$
Heat capacity	$(\rho C_p)_{nf} = (1 - \phi_1)(\rho C_p)_f + \phi_1(\rho C_p)_{n1}$
Viscosity	$\mu_{nf} = \frac{\mu_f}{(1 - \phi_1)^{2.5}}$
Thermal diffusivity	$\alpha_{nf} = \frac{k_{nf}}{(\rho C_p)_{nf}}$
Thermal conductivity	$\frac{k_{nf}}{k_f} = \frac{k_{n1} + 2k_f - 2\phi_1(k_f - k_{n1})}{k_{n1} + 2k_f + \phi_1(k_f - k_{n1})}$
Electrical conductivity	$\frac{\sigma_{nf}}{\sigma_f} = 1 + \frac{3\left(\frac{\sigma_{n1}}{\sigma_f} - 1\right)\phi_1}{2 + \frac{\sigma_{n1}}{\sigma_f} - \left(\frac{\sigma_{n1}}{\sigma_f} - 1\right)\phi_1}$

Table 3. Thermophysical properties of hybrid nanofluid (type II) [35].

Properties	Nanofluid
Density	$\rho_{hnf} = (1 - \phi_2)[(1 - \phi_1)\rho_f + \phi_1\rho_{n1}] + \phi_2\rho_{n2}$
Thermal expansion coefficient	$(\rho\beta)_{hnf} = (1 - \phi_2)[(1 - \phi_1)(\rho\beta)_f + \phi_1(\rho\beta)_{n1}] + \phi_2(\rho\beta)_{n2}$
Heat capacity	$(\rho C_p)_{hnf} = (1 - \phi_2)[(1 - \phi_1)(\rho C_p)_f + \phi_1(\rho C_p)_{n1}] + \phi_2(\rho C_p)_{n2}$
Viscosity	$\mu_{hnf} = \frac{\mu_f}{(1 - \phi_1)^{2.5}(1 - \phi_2)^{2.5}}$
Thermal diffusivity	$\alpha_{hnf} = \frac{k_{hnf}}{(\rho C_p)_{hnf}}$
Thermal conductivity	$\frac{k_{hnf}}{k_{nf}} = \frac{k_{n2} + 2k_{nf} - 2\phi_2(k_{nf} - k_{n2})}{k_{n2} + 2k_{nf} + \phi_2(k_{nf} - k_{n2})}$, where $\frac{k_{nf}}{k_f} = \frac{k_{n1} + 2k_f - 2\phi_1(k_f - k_{n1})}{k_{n1} + 2k_f + \phi_1(k_f - k_{n1})}$
Electrical conductivity	$\frac{\sigma_{hnf}}{\sigma_{nf}} = \frac{\sigma_{n2} + 2\sigma_{nf} - 2\phi_2(\sigma_{nf} - \sigma_{n2})}{\sigma_{n2} + 2\sigma_{nf} + \phi_2(\sigma_{nf} - \sigma_{n2})}$, where $\frac{\sigma_{nf}}{\sigma_f} = \frac{\sigma_{n1} + 2\sigma_f - 2\phi_1(\sigma_f - \sigma_{n1})}{\sigma_{n1} + 2\sigma_f + \phi_1(\sigma_f - \sigma_{n1})}$

Table 4. Thermophysical properties of hybrid nanofluid (type III) [36,37].

Properties	Nanofluid
Density	$\rho_{hnf} = (1 - \phi_1 - \phi_2)\rho_f + \phi_1\rho_{n1} + \phi_2\rho_{n2}$
Thermal expansion coefficient	$(\rho\beta)_{hnf} = (1 - \phi_1 - \phi_2)(\rho\beta)_f + \phi_1(\rho\beta)_{n1} + \phi_2(\rho\beta)_{n2}$
Heat capacity	$(\rho C_p)_{hnf} = (1 - \phi_1 - \phi_2)(\rho C_p)_f + \phi_1(\rho C_p)_{n1} + \phi_2(\rho C_p)_{n2}$
Viscosity	$\mu_{hnf} = \frac{\mu_f}{(1 - \phi_1 - \phi_2)^{2.5}}$
Thermal diffusivity	$\alpha_{hnf} = \frac{k_{hnf}}{(\rho C_p)_{hnf}}$
Thermal conductivity	$\frac{k_{hnf}}{k_{nf}} = \frac{k_{n2} + 2k_{nf} - 2\phi_2(k_{nf} - k_{n2})}{k_{n2} + 2k_{nf} + \phi_2(k_{nf} - k_{n2})}$, where $\frac{k_{nf}}{k_f} = \frac{k_{n1} + 2k_f - 2\phi_1(k_f - k_{n1})}{k_{n1} + 2k_f + \phi_1(k_f - k_{n1})}$
Electrical conductivity	$\frac{\sigma_{hnf}}{\sigma_{nf}} = \frac{\sigma_{n2} + 2\sigma_{nf} - 2\phi_2(\sigma_{nf} - \sigma_{n2})}{\sigma_{n2} + 2\sigma_{nf} + \phi_2(\sigma_{nf} - \sigma_{n2})}$, where $\frac{\sigma_{nf}}{\sigma_f} = \frac{\sigma_{n1} + 2\sigma_f - 2\phi_1(\sigma_f - \sigma_{n1})}{\sigma_{n1} + 2\sigma_f + \phi_1(\sigma_f - \sigma_{n1})}$

Introduce the following dimensionless variables

$$\begin{aligned}
 X &= \alpha_f x / (\bar{u} L^2), \quad Y = y / L, \quad U(Y) = u / \bar{u}, \\
 \theta(X, Y) &= (T - T_0) / (qL / k_f), \\
 P(X, Y) &= \left[p - \rho_f g (x \sin \gamma - y \cos \gamma) \right] / (\text{Pr} \rho_f \bar{u}^2), \tag{6}
 \end{aligned}$$

where α_f is the thermal diffusivity of the base fluid, ν_f is the kinematic viscosity of the base fluid, $\text{Pr} = \nu_f / \alpha_f$ is the Prandtl number. Substituting variables (6) into Equations (1)–(3), the following dimensionless equations are obtained

$$\frac{\partial P}{\partial X} = -P_1 \frac{(\rho\beta)_{hmf}}{(\rho\beta)_f} \theta + \frac{\mu_{hmf}}{\mu_f} \frac{d^2 U}{dY^2}, \quad (7)$$

$$\frac{\partial P}{\partial Y} = P_2 \frac{(\rho\beta)_{hmf}}{(\rho\beta)_f} \theta, \quad (8)$$

$$U \frac{\partial \theta}{\partial X} = \frac{\alpha_{hmf}}{\alpha_f} \frac{\partial^2 \theta}{\partial Y^2}, \quad (9)$$

subject to the boundary conditions

$$U(0) = 0, \quad U(1) = 0, \quad -\left(\frac{\partial \theta}{\partial Y}\right)_{Y=0} = \left(\frac{\partial \theta}{\partial Y}\right)_{Y=1} = 1, \quad (10)$$

along with the mass flux conservation relation

$$\int_0^1 U dY = 1. \quad (11)$$

Here $P_1 = Gr \sin \gamma / Re$ and $P_2 = Gr \cos \gamma / (Pr Re^2)$ are nondimensional pressure parameters, $Gr = g\beta_f q L^4 / (k_f \nu_f^2)$ is the Grashof number and $Re = \bar{u}L / \nu_f$ is the Reynolds number.

Integrating Equation (9) over the channel cross-section, making use of Equation (11) and the boundary conditions (10) for temperature distribution θ , and considering the constant heat flux distribution of x -direction at the walls, the following relation can be obtained

$$\frac{\partial \theta}{\partial X} = 2 \frac{\alpha_{hmf}}{\alpha_f}. \quad (12)$$

Differentiating Equation (7) with Y and Equation (8) with X respectively, and taking into account (12), then equating them, we obtain

$$-P_1 \frac{(\rho\beta)_{hmf}}{(\rho\beta)_f} \frac{\partial \theta}{\partial Y} + \frac{\mu_{hmf}}{\mu_f} \frac{d^3 U}{dY^3} = 2 \frac{\alpha_{hmf}}{\alpha_f} \frac{(\rho\beta)_{hmf}}{(\rho\beta)_f} P_2. \quad (13)$$

Differentiating this equation with Y once again, we obtain

$$\frac{\mu_{hmf}}{\mu_f} \frac{d^4 U}{dY^4} = P_1 \frac{(\rho\beta)_{hmf}}{(\rho\beta)_f} \frac{\partial^2 \theta}{\partial Y^2}. \quad (14)$$

Making use of Equations (9) and (12), we finally obtain

$$\frac{\mu_{hmf}}{\mu_f} \frac{d^4 U}{dY^4} = 2P_1 \frac{(\rho\beta)_{hmf}}{(\rho\beta)_f} U. \quad (15)$$

This equation can be solved analytically for the velocity distribution U , the temperature distribution θ and the pressure distribution P can be determined as well. The analytical solution of Equation (15) can be obtained by using the computational softwares such as MATHEMATICA or MAPLE.

Using the software MATHEMATICA and taking account of the boundary conditions (10), the analytical solutions of the velocity distribution U , the temperature distribution θ and the pressure distribution P can be given explicitly as

$$U(Y) = a[\sinh(mY) + \sin(mY)] + b[\cosh(mY) - \cos(mY)] + c \sin(mY), \quad (16)$$

$$\theta(X, Y) = \frac{2}{m^2} \{ a[\sinh(mY) - \sin(mY)] + b[\cosh(mY) + \cos(mY)] - c \sin(mY) \} - \frac{2P_2}{P_1} \frac{\alpha_{hnf}}{\alpha_f} Y + 2 \frac{\alpha_{hnf}}{\alpha_f} X + A, \quad (17)$$

$$P(X, Y) = \frac{(\rho\beta)_{hnf}}{(\rho\beta)_f} \left\{ \frac{2P_2}{m^3} \{ a[\cosh(mY) + \cos(mY)] + b[\sinh(mY) + \sin(mY)] + c \cos(mY) \} + P_2 \left(2 \frac{\alpha_{hnf}}{\alpha_f} XY + AY - \frac{P_2}{P_1} \frac{\alpha_{hnf}}{\alpha_f} Y^2 \right) - P_1 \left(AX + \frac{\alpha_{hnf}}{\alpha_f} X^2 \right) + B \right\}, \quad (18)$$

where A and B are the constants, whose values are dependent on the given values of P_1 and P_2 , and they must satisfy the boundary conditions for θ and P . The parameters a, b, c and m are given as

$$\begin{aligned} a &= \frac{[m - c + c \cos(m)][\cosh(m) - \cos(m)]}{-2[\cosh(m) \cos(m) - 1]} + \frac{c \sin(m)[\sinh(m) - \sin(m)]}{-2[\cosh(m) \cos(m) - 1]}, \\ b &= \frac{[m - c + c \cos(m)][\sinh(m) + \sin(m)]}{2[\cosh(m) \cos(m) - 1]} + \frac{c \sin(m)[\cosh(m) - \cos(m)]}{2[\cosh(m) \cos(m) - 1]}, \\ c &= m \left(\frac{1}{2} - \frac{P_2}{P_1} \frac{\alpha_{hnf}}{\alpha_f} \right), \quad m^4 = 2P_1 \frac{(\rho\beta)_{hnf}}{(\rho\beta)_f} \frac{\mu_f}{\mu_{hnf}}. \end{aligned} \quad (19)$$

Once the values of P_1 and P_2 are artificially prescribed, the analytical solutions of U , θ and P can be fully determined. Note that the analytical solution for the horizontal case ($P_1 = 0$) can be obtained by expanding the above solutions for small m , or more simply, by solving the Equations (7)–(9) by setting $P_1 = 0$. Noting that for $\phi_1 = \phi_2 = 0$, the solutions are reduced to those of Lavine [7].

The physical quantities of practical interest in this problem are the wall friction $C_f Re$ and the Nusselt number Nu , they are given by

$$C_f Re = \frac{\tau_w}{\frac{1}{2} \rho_f \bar{u}^2} \frac{\bar{u} L}{\nu_f}, \quad Nu = \frac{2 q L}{k_f (T_w - T_b)}, \quad (20)$$

where T_w is the wall temperature, T_b is the bulk temperature. τ_w is the wall shear stress which is defined by

$$\tau_w = \pm \mu_{nf} \left. \frac{\partial u}{\partial y} \right|_{0,L}, \quad (21)$$

where \pm signs correspond to the bottom and top walls, respectively.

Substituting Equations (6) and (21) into Equation (20), we obtain

$$C_f Re = \begin{cases} 2m \frac{\mu_{hnf}}{\mu_f} (2a + c) & \text{at } Y = 0, \\ -2m \frac{\mu_{hnf}}{\mu_f} \left\{ a[\cosh(m) + \cos(m)] + b[\sinh(m) + \sin(m)] + c \cos(m) \right\} & \text{at } Y = 1, \end{cases} \quad (22)$$

and

$$Nu = \frac{2qL}{k_f(T_w - T_b)} = \frac{2}{(\theta_w - \theta_b)}, \quad (23)$$

where

$$\theta_b = \int_0^1 U\theta dY \quad \text{and} \quad \theta_w = \theta(Y = 0, 1). \quad (24)$$

The average of the top and bottom wall friction is also of interest. It is given by:

$$\begin{aligned} \overline{C_f Re} &= \frac{1}{2}[C_f Re(Y = 0) + C_f Re(Y = 1)] \\ &= \frac{\mu_{hnf} m^2 [\cos(m) - \cosh(m) - \sin(m) \sinh(m)]}{\mu_f \cos(m) \cosh(m) - 1}. \end{aligned} \quad (25)$$

Thus, the average wall friction ($\overline{C_f Re}$) is seen to be independent of parameter P_2 . Similarly, the average of the top and bottom Nusselt number is given by:

$$\begin{aligned} \overline{Nu} &= \frac{1}{2}[Nu(Y = 0) + Nu(Y = 1)] \\ &= \frac{1}{\theta_w|_{Y=0} - \theta_b} + \frac{1}{\theta_w|_{Y=1} - \theta_b}. \end{aligned} \quad (26)$$

Furthermore, the average Nusselt number (\overline{Nu}) is dependent of parameter P_2 .

3. Results and Discussion

To comprehend the current problem, the physical influence of the governing parameters, such as the pressure parameters P_1, P_2 , the nanoparticle volume fractions ϕ_1, ϕ_2 , the velocity profile $U(Y)$, the temperature profile $\theta - \theta_b$, the average wall friction $\overline{C_f Re}$ and the average Nusselt number \overline{Nu} are illustrated graphically. The flow reversal occurs to the upper wall satisfies $(dU/dY)|_{Y=1} = 0$, or $C_f Re|_{Y=1} = 0$. The following constraint relationship of P_1 and P_2 based on Equation (22) can be obtained as

$$\frac{\alpha_{hnf}}{\alpha_f} P_2 = \frac{P_1 \cos(m) - \cosh(m) - \sin(m) \sinh(m)}{2 \cos(m) - \cosh(m) + \sin(m) \sinh(m)}. \quad (27)$$

The flow regime map of the base fluid (H_2O), nanofluid ($Cu-H_2O$, type I) and hybrid nanofluid ($Cu-Al_2O_3-H_2O$, type II and III) with ϕ_1, ϕ_2 , the inflexion exists for each curve with corresponding to $P_2 = 0$ and $P_1 = P_{1,c}$ is shown in Figure 2 and Table 5. About the base fluid, nanofluid and hybrid nanofluid, $P_{1,c}$ is the critical value for P_1 which value is 250.281948 (Lavine's case [7]) for $\phi_1 = \phi_2 = 0$. For $P_1 \leq P_{1,c}$, the involved region is divided into two parts by a certain curve. The upper part is the regime that the flow reversal occurs to the top wall only, and the lower part is the regime in which no flow reversal can be measured. For $P_1 \geq P_{1,c}$, this curve separates the regime for which flow reversal occurs to both walls of the regime of flow reversal of the bottom wall only. For a vertical channel ($P_2 = 0$), flow reversal must occur to both walls of the flow in symmetric about the channel centerline in this configuration. About the nanofluid, $P_{1,c} = 288.675450$ for $\phi_1 = 0.05$ and $P_{1,c} = 335.346949$ for $\phi_1 = 0.1$. Furthermoer, the hybrid nanofluid, $P_{1,c} = 342.496247$ (type II) and $P_{1,c} = 345.142372$ (type III) for $\phi_1 = \phi_2 = 0.05$; $P_{1,c} = 476.114704$ (type II) and $P_{1,c} = 492.724576$ (type III) for $\phi_1 = \phi_2 = 0.1$, respectively. For a horizontal channel ($P_1 = 0$), it is expected that the occurrence of flow reversal of upper wall is founded for $P_2 > P_{2,c}$, where $P_{2,c}$ is the critical value of P_2 with its value. With $\phi_1 = \phi_2 = 0$, $P_{2,c} = 35.999978$ with the base fluid, $P_{2,c} = 35.972464$ with the nanofluid and hybrid nanofluid. About nanofluid, $P_{2,c} = 35.543514$ for $\phi_1 = 0.05$ and $P_{2,c} = 35.562942$ for $\phi_1 = 0.1$. And hybrid nanofluid, $P_{2,c} = 36.203632$ (type II) and $P_{2,c} = 36.467267$ (type III) for $\phi_1 = \phi_2 = 0.05$; $P_{2,c} = 37.499401$ (type II) and $P_{2,c} = 38.736813$ (type III) for $\phi_1 = \phi_2 = 0.1$, respectively. With increasing from ϕ_1, ϕ_2 , the critical values $P_{1,c}$ enlarges simultaneously. Notice that $P_{1,c}$ enlarges on increasing ϕ_1, ϕ_2 , while $P_{2,c}$ also increases. Results show that the nanoparticle volume fractions ϕ_1, ϕ_2 play a key role in delaying the occurrence of the flow reversal. The

hybrid nanofluids hold more delayed range than conventional nanofluids, which is about 2.5 times that of nanofluids. The calculations of hybrid nanofluid about type II and type III agree very well; the relative error compared with hybrid nanofluid of type II is 0.7% for $\phi_1 = \phi_2 = 0.05$ and 3% for $\phi_1 = \phi_2 = 0.1$. So the hybrid nanofluid of type III that is proposed based on the linear assumptions is useful.

Table 5. The critical values of P_1 and P_2 .

Critical Values	Types	$\phi_1 = \phi_2 = 0$	$\phi_1 = \phi_2 = 0.05$	$\phi_1 = \phi_2 = 0.1$
$P_{1,c}$	H_2O (Lavine's case [7])	250.281948	-	-
	$Cu-H_2O$ (type I)	250.281948	288.675450	335.346949
	$Al_2O_3-H_2O$ [12]	250.281948	296.981071	355.527252
	$Cu-Al_2O_3-H_2O$ (type II)	250.281948	342.496247	476.114704
	$Cu-Al_2O_3-H_2O$ (type III)	250.281948	345.142372	492.724576
$P_{2,c}$	H_2O (Lavine's case [7])	35.999978	-	-
	$Cu-H_2O$ (type I)	35.972464	35.543514	35.562942
	$Al_2O_3-H_2O$ [12]	35.972464	36.597696	37.750800
	$Cu-Al_2O_3-H_2O$ (type II)	35.972463	36.203632	37.499401
	$Cu-Al_2O_3-H_2O$ (type III)	35.972463	36.467267	38.736813

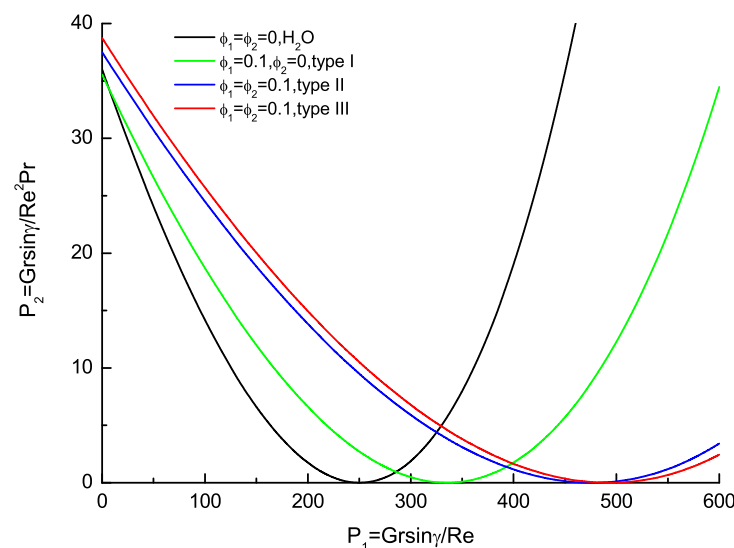


Figure 2. Flow regime map of the base fluid (H_2O), nanofluid ($Cu-H_2O$, type I) and hybrid nanofluid ($Cu-Al_2O_3-H_2O$, type II and III).

Velocity and temperature profiles for the base fluid, nanofluid and hybrid nanofluid are presented in Figures 3 and 4. The velocity and temperature profiles for the liquid at $P_1=100$ with $P_2 = 0$ and $P_2 = 36$ have been analyzed and temperature profiles will be illustrated as $\theta - \theta_b$ that eliminate the x -dependence. The velocity profiles are symmetric about the centerline and no flow reversals are found for all considered ϕ_1, ϕ_2 for $P_2 = 0$ corresponding to the vertical channel configuration. The velocity near the walls increases as ϕ_1, ϕ_2 increase, while the velocity in the vicinity of the centerline decreases from ϕ_1, ϕ_2 increasing. The effects of ϕ_1, ϕ_2 on the velocity distribution are evident; the increases in ϕ_1, ϕ_2 delay the velocity reduction near the upper wall compared with the base fluid, nanofluid and hybrid nanofluid. Furthermore, the calculations of hybrid nanofluid about type II and type III agree very well. In the case of $P_2 = 36$, for any given values of ϕ_1, ϕ_2 , it is found that the velocity peak enlarges in magnitude and moves to the lower wall ($Y = 0$) compared with $P_2 = 0$, while the velocity near the upper wall ($Y = 1$) decreases with the flow reversal. The temperature profiles for the base fluid, nanofluid and hybrid nanofluid at $P_1 = 100$ are presented in Figure 4. The temperature near the upper wall

increases accordingly as P_2 enlarges. At the same time, the valley of the temperature shifts towards the lower wall and its value increases consecutively with the increase in P_2 . The temperature variation near the upper wall becomes larger and larger and the valley of the temperature moves to the upper wall gradually as ϕ_1, ϕ_2 increase for P_2 . The hybrid nanofluids about type II and type III agree very well, which are potential fluids that offer better thermophysical properties and heat transfer performance than convective fluids and nanofluids with single nanoparticles.

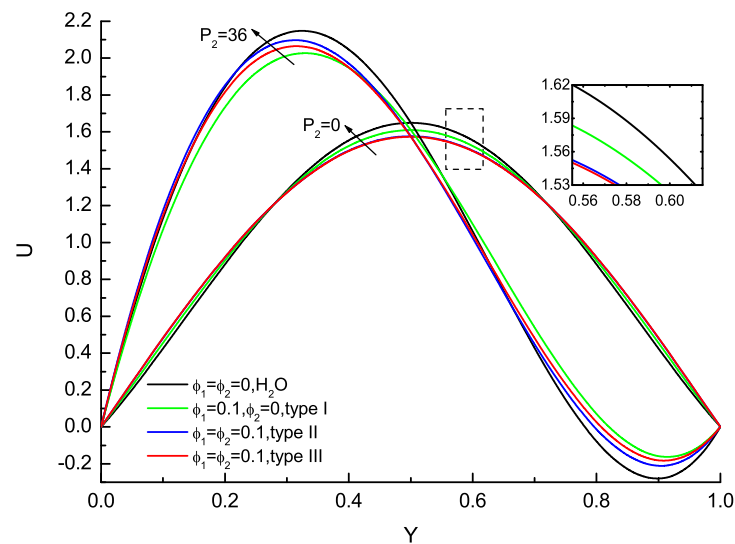


Figure 3. Variation with P_2 of the velocity profiles for the base fluid (H_2O), nanofluid ($Cu-H_2O$, type I) and hybrid nanofluid ($Cu-Al_2O_3-H_2O$, type II & III) at $P_1 = 100$.

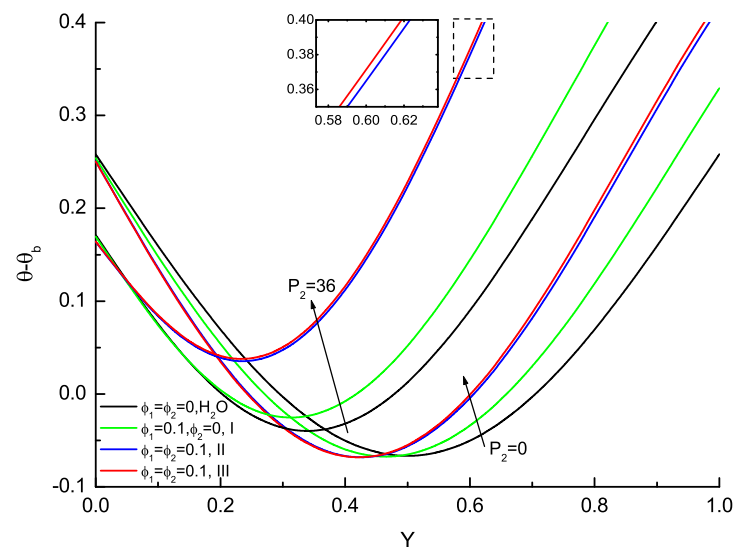


Figure 4. Variation with P_2 of the temperature profiles for the base fluid (H_2O), nanofluid ($Cu-H_2O$, type I) and hybrid nanofluid ($Cu-Al_2O_3-H_2O$, type II & III) at $P_1 = 100$.

The average wall friction $\overline{C_f Re}$ and the average Nusselt number \overline{Nu} are also physical quantities of practical interests, as shown as Figures 5 and 6. Figure 5 shows the effects of ϕ_1, ϕ_2 on the average wall friction with the base fluid, nanofluid and hybrid nanofluid. The average wall friction that is the independent of parameter P_2 decreases monotonously as P_1 increases. The hybrid nanofluids about type II and type III agree very well as P_1 increases, and the relative error compared with hybrid nanofluid of type II is 3% for $\phi_1 = \phi_2 = 0.1$. Figure 6 shows the effects of ϕ_1, ϕ_2 on the average Nusselt number with the

base fluid, nanofluid and hybrid nanofluid. Contrary to the average friction, the average Nusselt number is dependent of P_2 and its value is equal to the average of top and bottom Nusselt number for P_1, P_2 and ϕ_1, ϕ_2 are prescribed. The average Nusselt number increases monotonously with the base fluid, nanofluid and hybrid nanofluid as P_1 increases for $P_2 = 0$. At the same time, the valley of the average Nusselt number shifts towards the lower wall and its value increases consecutively with the increase in P_2 . The effects of ϕ_1, ϕ_2 on the average Nusselt number distribution are evident with the base fluid, nanofluid and hybrid nanofluid. Furthermore, the calculations of hybrid nanofluid about type II and type III are in very good agreement. The hybrid nanofluids are potential fluids that offer better thermophysical properties and heat transfer performance than convectual fluids and nanofluids with single nanoparticles.

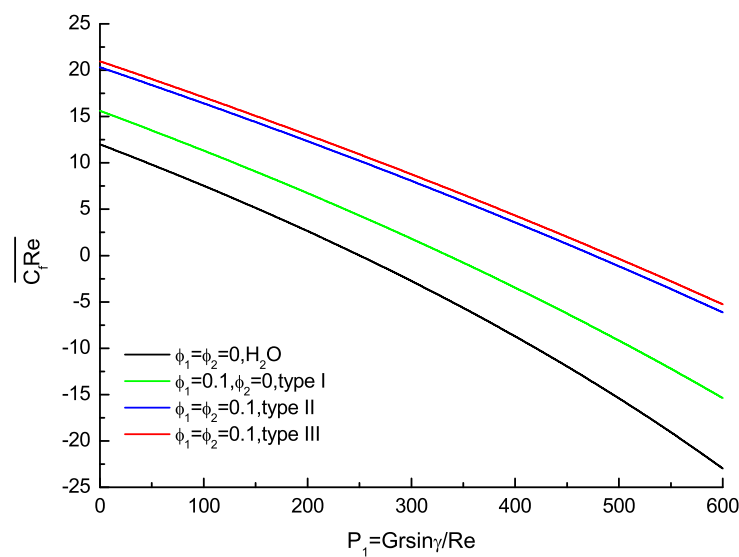


Figure 5. Variation of average $C_f Re$ with P_1 when $Re = 10, Pr = 1$ and $Gr = 3000$.

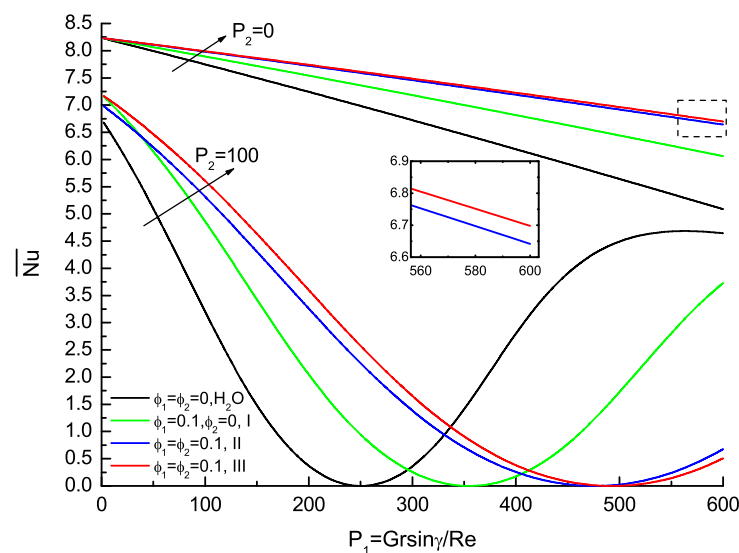


Figure 6. Variation of average Nu with P_1 for $P_2 = 0$ and $P_2 = 100$ when $Re = 10, Pr = 1$ and $Gr = 3000$.

4. Conclusions

In this paper, fully developed mixed convection flow in the inclined channel filled by a hybrid nanofluid with a uniform wall heat flux boundary condition has been studied. The governing ordinary differential equations are made nondimensional and they are solved analytically. The explicitly analytical solutions of the velocity, temperature and pressure have been given. The effects of flow reversal, wall skin friction and Nusselt number of the hybrid nanofluid that depend on the nanoparticle volume fractions and pressure parameters are discussed and shown graphically (see Section 3). The hybrid nanofluids are potential fluids that offer better thermophysical properties and heat transfer performance than convectional fluids and nanofluids with single nanoparticles. The main key findings are listed below.

- (1) The nanoparticle volume fractions play a key role in delaying the occurrence of the flow reversal. The hybrid nanofluids hold a more delayed range than conventional nanofluids, which is about 2.5 times that of nanofluids.
- (2) Two hybrid models (type II and type III) are compared with different nanoparticle volume fractions ϕ_1, ϕ_2 and pressure parameters P_1, P_2 . It is observed that they are in very good agreement, with the relative error less than 3%. The hybrid model of type III is useful and simplified in that it omits the nonlinear terms due to the interaction of different nanoparticle volumetric fractions.
- (3) The effects of nanoparticle volume fractions on the velocity and temperature distributions are evident, the increases of ϕ_1, ϕ_2 delay the velocity reduction and enlarge the temperature variation near the upper wall ($Y = 1$) compared with the base fluid, nanofluid and hybrid nanofluid.
- (4) The average wall friction ($\overline{C_f Re}$) that is independent of P_2 decreases monotonously as P_1 increases. The average Nusselt number (\overline{Nu}) that is dependent of P_2 increases monotonously as P_1 increases for the vertical channel ($P_2 = 0$). The valley of the average Nusselt number shifts towards the lower wall and its value increases consecutively with the increase of P_2 .

Author Contributions: X.Y.; original draft preparation, software, formal analysis, S.L.; supervision, project administration. All authors have read and agreed to the published version of the manuscript.

Funding: This work is supported by the National Natural Science Foundation of China (Grant No. 12002390 and 51704307) and Foundation of China University of Petroleum-Beijing (ZX20200119).

Institutional Review Board Statement: Not applicable.

Informed Consent Statement: Not applicable.

Data Availability Statement: All drawings were made by myself.

Acknowledgments: We thank the anonymous referees for their valuable comments and discussions.

Conflicts of Interest: The authors declare no conflict of interest.

Nomenclature

The following nomenclature is used in this manuscript:

A, B	Constants
C_f	Wall skin friction coefficient
$\overline{C_f}$	Average wall skin friction
C_p	Specific heat at constant pressure
g	Acceleration due to gravity
Gr	Grashof number
k_{hnf}	Thermal conductivity of the hybrid nanofluid
k_f, k_n	Thermal conductivities of the base fluid and nanofluid, respectively

L	Distance between the walls
Nu	Nusselt number
p	Dimensional thermodynamic pressure
P	Dimensionless thermodynamic pressure
P_1, P_2	Dimensionless pressure parameters
$P_{1,c}, P_{2,c}$	Critical values for P_1 and P_2 , respectively
Pr	Prandtl number
q	Constant wall heat flux
Re	Reynolds number
T	Nanofluid temperature
T_b, T_w	Bulk and wall temperature, respectively
T_0	Constant reference temperature
$u(y)$	Dimensional velocity component along the x axis
\bar{u}	Dimensional average velocity
$U(Y)$	Dimensionless velocity component along the X axis
x	Dimensional axis measured along lower plane of channel oriented in downward direction
y	Dimensional axis measured in the normal direction to the lower plane
X, Y	Dimensionless coordinates
α_{hmf}	Thermal diffusivity of the hybrid nanofluid
α_f	Thermal diffusivity of the base fluid
β_f, β_n	Coefficients of thermal expansion of the fluid and nanofluid, respectively
ϕ_1, ϕ_2	Nanoparticle volume fractions
γ	Inclination of the channel
μ_{hmf}	Viscosity of the hybrid nanofluid
μ_f	Dynamic viscosity of the base fluid
ν_f	Kinematic viscosity of the base fluid
θ	Dimensionless nanofluid temperature
θ_b, θ_w	Dimensionless bulk and wall temperature, respectively
$(\rho C_p)_{hmf}$	Heat capacitance of the hybrid nanofluid
ρ_f, ρ_n	Densities of the fluid and nanofluid fractions, respectively
τ_w	Skin friction or wall shear stress

References

1. Chang, T.S.; Lin, T.F. Steady and oscillatory opposing mixed convection in a symmetrically heated vertical channel with a low-Prandtl number fluid. *Int. J. Heat Mass Transf.* **1993**, *36*, 3783–3795.
2. Barletta, A. Dual mixed convection flows in a vertical channel. *Int. J. Heat Mass Transf.* **2005**, *48*, 4835–4845. [[CrossRef](#)]
3. Chang, T.S. Effects of a finite section with linearly varying wall temperature on mixed convection in a vertical channel. *Int. J. Heat Mass Transf.* **2007**, *50*, 2346–2354. [[CrossRef](#)]
4. Xu, H.; Pop, I. Fully developed mixed convection flow in a vertical channel filled with nanofluids. *Int. Comm. Heat Mass Transf.* **2012**, *39*, 1086–1092. [[CrossRef](#)]
5. Jamaludin, A.; Naganthran, K.; Nazar, R.; Pop, I. MHD mixed convection stagnation-point flow of $Cu-Al_2O_3$ /water hybrid nanofluid over a permeable stretching/shrinking surface with heat source/sink. *Eur. J. Mech./B Fluids* **2020**, *84*, 71–80. [[CrossRef](#)]
6. Bohne, D.; Obermeier, E. Combined free and forced convection in a vertical and inclined cylindrical annulus. In *International Heat Transfer Conference Digital Library*; Begel House Inc.: Danbury, CT, USA, 1986; Volume 3, pp. 1401–1406.
7. Lavine, A.S. Analysis of fully developed opposing mixed convection between inclined parallel plates. *Heat Mass Transf.* **1988**, *23*, 249–257. [[CrossRef](#)]
8. Wang, X. Mixed convection in an inclined channel with localized heat sources. *Num. Heat Tran. A Appl.* **1995**, *28*, 355–373. [[CrossRef](#)]
9. Barletta, A.; Zanchini, E. Mixed convection with viscous dissipation in an inclined channel with prescribed wall temperatures. *Int. J. Heat Mass Transf.* **2001**, *44*, 4267–4275. [[CrossRef](#)]
10. Aydin, O.; Kaya, A. MHD mixed convective heat transfer flow about an inclined plate. *Heat Mass Transf.* **2009**, *46*, 129–136. [[CrossRef](#)]
11. Cimpean, D.S.; Pop, I. Fully developed mixed convection flow of a nanofluid through an inclined channel filled with a porous medium. *Int. J. Heat Mass Transf.* **2012**, *55*, 907–914. [[CrossRef](#)]
12. You, X.Y.; Xu, H. Analysis of fully developed opposing mixed convection flow in an inclined channel filled by a nanofluid. *J. Heat Transf.* **2014**, *136*, 124502. [[CrossRef](#)]

13. Goyal, M.; Bhargava, R. Simulation of natural convective boundary layer flow of a nanofluid past a convectively heated inclined plate in the presence of magnetic field. *Int. J. Appl. Comput. Math.* **2018**, *4*, 63. [[CrossRef](#)]
14. Rafique, K.; Anwar, M.I.; Misiran, M. Numerical study on micropolar nanofluid flow over an inclined surface by means of keller-box. *Asian J. Probab. Stat.* **2019**, *4*, 1–21. [[CrossRef](#)]
15. Khademi, R.; Razminia, A.; Shiryaev, V.I. Conjugate-mixed convection of nanofluid flow over an inclined flat plate in porous media. *Appl. Math. Comput.* **2020**, *366*, 124761. [[CrossRef](#)]
16. Anuar, N.S.; Bachok, N.; Pop, I. Influence of buoyancy force on Ag-MgO/water hybrid nanofluid flow in an inclined permeable stretching/shrinking sheet. *Int. Commun. Heat Mass Transf.* **2021**, *123*, 105236. [[CrossRef](#)]
17. Choi, S.; Eastman, J.A. Enhancing thermal conductivity of fluids with nanoparticle in developments and applications of Non-Newtonian Flows. *ASME Fluids Eng. Div.* **1995**, *231*, 99–105.
18. Esfe, M.H.; Saedodin, S.; Biglari, M.; Rostamian, H. Experimental investigation of thermal conductivity of CNTs- Al_2O_3 /water: A statistical approach. *Int. Commun. Heat Mass Transf.* **2015**, *69*, 29–33. [[CrossRef](#)]
19. Aberoumand, S.; Jafarimoghaddam, A.; Moravej, M.; Aberoumand, H.; Javaherdeh, K. Experimental study on the rheological behavior of silver-heat transfer oil nanofluid and suggesting two empirical based correlations for thermal conductivity and viscosity of oil based nanofluids. *Appl. Therm. Eng.* **2016**, *101*, 362–372. [[CrossRef](#)]
20. Yang, L.; Xu, J.; Du, K.; Zhang, X. Recent developments on viscosity and thermal conductivity of nanofluids. *Powder Tech.* **2017**, *317*, 348–369. [[CrossRef](#)]
21. Pramuanjaroenkij, A.; Tongkratoke, A.; Kaka, S. Numerical study of mixing thermal conductivity models for nanofluid heat transfer enhancement. *J. Eng. Phys. Therm.* **2018**, *91*, 104–114. [[CrossRef](#)]
22. Esfe, M.H. On the evaluation of the dynamic viscosity of non-Newtonian oil based nanofluids. *J. Therm. Anal. Calorim.* **2019**, *135*, 97–109. [[CrossRef](#)]
23. Mohebbifar, M.; Ghazanfari, M.H.; Vossoughi, M. Experimental investigation of nanobiomaterial applications for heavy oil recovery in shaly porous models: a pore-level study. *J. Energy Resour. Tech.* **2015**, *137*, 014501. [[CrossRef](#)]
24. Esfe, M.H.; Hosseinzadeh, E.; Esfandeh, S. Flooding numerical simulation of heterogeneous oil reservoir using different nanoscale colloidal solutions. *J. Mol. Liq.* **2020**, *302*, 111972. [[CrossRef](#)]
25. Nabil, M.F.; Azmi, W.H.; Hamid, K.A.; Zawawi, N.N.M.; Priyandoko, G.; Mamat, R. Thermo-physical properties of hybrid nanofluids and hybrid nanolubricants: A comprehensive review on performance. *Int. Commun. Heat Mass Transf.* **2017**, *83*, 30–39. [[CrossRef](#)]
26. Babu, J.R.; Kumar, K.K.; Rao, S.S. State-of-art review on hybrid nanofluids. *Renew. Sustain. Energy Rev.* **2017**, *77*, 551–565. [[CrossRef](#)]
27. Salman, S.; Talib, A.R.A.; Sultan, M.T.H. Hybrid nanofluid flow and heat transfer over backward and forward steps: A review. *Powder Tech.* **2020**, *363*, 448–472. [[CrossRef](#)]
28. Wainia, I.; Ishakb, A.; Pop, I. Flow and heat transfer of a hybrid nanofluid past a permeable moving surface. *Chin. J. Phys.* **2020**, *66*, 606–619. [[CrossRef](#)]
29. Khan, U.; Wainia, I.; Ishak, A.; Pop, I. Steady and oscillatory opposing mixed convection in a symmetrically heated vertical channel with a low-Prandtl number fluid. *Int. J. Mol. Liq.* **2021**, *331*, 115752. [[CrossRef](#)]
30. Elsaied, E.M.; Abdel-wahed, M.S. Mixed convection hybrid-nanofluid in a vertical channel under the effect of thermal radiative flux. *Case Stud. Therm. Eng.* **2021**, *25*, 100913. [[CrossRef](#)]
31. Maïga, S.E.B.; Palm, S.J.; Nguyen, C.T.; Roy, G.; Galanis, N. Heat transfer enhancement by using nanofluids in forced convection flows. *Int. J. Heat Fluid Flow* **2005**, *26*, 530–546. [[CrossRef](#)]
32. Brinkman, H.C. The viscosity of concentrated suspensions and solutions. *J. Chem. Phys.* **1952**, *20*, 571–581. [[CrossRef](#)]
33. Oztop, H.F.; Abu-Nada, E. Numerical study of natural convection in partially heated rectangular enclosures filled with nanofluids. *Int. J. Heat Fluid Flow* **2008**, *29*, 1326–1336. [[CrossRef](#)]
34. Devi, S.S.U.; Devi, S.P.A. Heat transfer enhancement of Cu- Al_2O_3 /water hybrid nanofluid flow over a stretching sheet. *J. Nigerian Math. Soc.* **2017**, *36*, 419–433.
35. Wainia, I.; Ishakb, A.; Grosan, T.; Pop, I. Mixed convection of a hybrid nanofluid flow along a vertical surface embedded in a porous medium. *Int. Commun. Heat Mass Transf.* **2020**, *114*, 104565. [[CrossRef](#)]
36. Xu, H. Modelling unsteady mixed convection of a nanofluid suspended with multiple kinds of nanoparticles between two rotating disks by generalized hybrid model. *Int. Commun. Heat Mass Transf.* **2019**, *108*, 104275. [[CrossRef](#)]
37. Xu, H.; Sun, Q. Generalized hybrid nanofluid model with application of fully developed mixed convection nanofluid flow in a vertical microchannel. *Commun. Theor. Phys.* **2019**, *71*, 903–911. [[CrossRef](#)]